

## APPLICATION OF THE OBSTACLE VECTOR FIELD METHOD FOR TRAJECTORY PLANNING OF A PLANAR MANIPULATOR IN SIMULATED MICROGRAVITY

Tomasz RYBUS, Konrad ALEKSIEJUK, Fatina Liliana BASMADJI,  
Adam SIKORSKI

Centrum Badań Kosmicznych Polskiej Akademii Nauk (CBK PAN),  
Warsaw, Poland

e-mails: [trybus@cbk.waw.pl](mailto:trybus@cbk.waw.pl), [kaleksiejuk@cbk.waw.pl](mailto:kaleksiejuk@cbk.waw.pl), [fbasmadji@cbk.waw.pl](mailto:fbasmadji@cbk.waw.pl),  
[asikorski@cbk.waw.pl](mailto:asikorski@cbk.waw.pl)

**ABSTRACT.** Capture and removal of large space debris is needed to prevent the growth of the debris population in low Earth orbit. Capture of a non-cooperative object by a manipulator mounted on a chaser satellite requires collision-free trajectory of the manipulator. The obstacle vector field (OVF) method allows to solve the trajectory planning problem in difficult scenarios. The OVF method is based on a vector field that surrounds the obstacles and generates virtual forces that drive the manipulator around the obstacles. The original formulation of the OVF method allows to obtain the desired position of the gripper, but not the desired orientation. To perform the grasping manoeuvre, the gripper has to be positioned in a specific point and aligned with the grasping interface. In this paper, we propose a modification to the OVF method that allows to obtain the desired position and orientation of the gripper. Moreover, we investigate the practical applicability of the OVF method. The OVF method is demonstrated in experiments performed on a planar air-bearing microgravity simulator. The presented results prove that the OVF method can be applied for a real system operating in simulated microgravity conditions.

**Keywords:** collision-free trajectory planning, obstacle vector field (OVF) method, active debris removal (ADR), free-floating manipulator, planar air-bearing microgravity simulator

### 1. INTRODUCTION

Large population of defunct artificial objects in low Earth orbit, known as space debris, poses a serious threat to operational satellites (Murtaza et al., 2020). Removal of existing objects from orbit is needed to prevent the growth of the space debris population (Liou et al., 2010). Thus, the active debris removal (ADR) missions are proposed to capture and remove large space debris from orbit (Bonnal et al., 2013). The European Space Agency (ESA) was working on the e.Deorbit mission to demonstrate the ADR capabilities (Biesbroek et al., 2017). The Clearspace-1 mission is currently under development to capture and remove a selected object from orbit (Biesbroek et al., 2021). Grasping of a target object in-orbit will be the most challenging part of the proposed missions. Various techniques can be used to perform the capture operation (Shan et al., 2016). The most mature approach is based on the use of a gripper attached to a manipulator mounted on a chaser satellite. Such an approach



was proposed for the e.Deorbit mission (Estable et al., 2020). Advanced trajectory planning and control algorithms are required to perform the capture operation (Flores-Abad et al., 2014). The control system must take into account the influence of the manipulator motion on the state of the chaser satellite (Dubowsky and Papadopoulos, 1993). Moreover, the manipulator has to avoid collisions with the elements of the target object. Satellites are equipped with appendages (e.g. solar panels), which make the trajectory planning task difficult.

In this paper, we focus on the problem of collision-free trajectory planning of a manipulator mounted on a free-floating chaser satellite. A review of trajectory planning methods applicable for the considered in-orbit capture operation was presented by Rybus (2018). The planning is performed in a high-dimensional configuration space, as the configuration of the satellite-manipulator system is described not only by the angular positions of manipulator joints, but also by the position and orientation of the chaser. The proposed methods include variants of the Rapidly exploring Random Tree (RRT) algorithm (Benevides and Grassi, 2015; Rybus, 2020), the A\* algorithm (Gao et al. 2011), and various optimisation techniques (Misra and Bai, 2017; Wang et al., 2018; Rybus et al., 2022). However, these approaches have a high computational cost, which can be a problem due to limited resources of the chaser satellite on-board computer and the short time available for the capture operation. Moreover, the RRT algorithm is based on the random search of the configuration space and it is not deterministic, that is, a different solution is generated in each run. Due to these facts, the possibility of practical application of the aforementioned methods in the ADR missions is limited. Thus, other methods for trajectory planning are being sought.

One of the considered approaches is based on the artificial potential field (APF) method. In the APF method, the manipulator is considered as a particle that is moving in an artificial force field (Khatib, 1986). This force field is composed of the attracting potential of the desired final position of the gripper and the repulsive potential of the obstacles. The APF method is widely used for fixed-base manipulators working on Earth (Lin and Chuang, 2003) and for mobile robots (Kowalczyk et al., 2012). Application of the APF method for a manipulator mounted on a chaser satellite was proposed by Mukherjee and Nakamura (1991). The existence of local minima of the potential field is the main disadvantage of the APF method (Park and Lee, 2003). The trajectory planning fails when the manipulator encounters a local minimum of the field. Yanoshita and Tsuda (2009) considered the trajectory planning problem for a satellite-manipulator system and proposed the potential field based on the Laplace function that allows to partially overcome the problem of local minima. Rybus and Seweryn (2018) modified the classical APF method by introducing a new approach for selection of the direction in which the repulsive force is acting. The modified APF method is more efficient than the classical APF method, that is, it allows to solve the trajectory planning problem in some of the cases, in which the classical APF method is unsuccessful.

Recently, Rybus (2022) proposed the obstacle vector field (OVF) method. In the classical APF method, a scalar potential field is used, while in the OVF method, a vector field is constructed. This vector field surrounds the obstacles and determines the direction in which the link of the manipulator should move to avoid collision with obstacles. The OVF method takes into account the fact that the motion of the manipulator influences the state of the chaser satellite. The OVF method is less efficient than the RRT algorithm, but it is more efficient than the modified APF method. Moreover, it is fully deterministic and it requires significantly less computational time than the RRT algorithm. The OVF method is, to some extent, similar to several concepts known from the literature. Masoud and Al-Shaikhi (2015) proposed an approach in which a vector field guides a mobile robot to the desired position. This field is produced from the harmonic potential and is perturbed by obstacles. The desired trajectory is

obtained by solving a gradient dynamical system. Such an approach is more complicated than the OVF method because the algorithm is based on partial differential equations. A trajectory planning algorithm based on parametrised vector potential functions was proposed by Pamosoaji and Hong (2013) for a unicycle vehicle. In this approach, the workspace is split into predefined triangular regions and the vector potential functions are calculated using information on regions' vertices, the obstacles, and the desired position of the vehicle. Masoud and Bayoumi (1993) used vector potential field for planning a trajectory of a fixed-base manipulator. The guiding vector field is generated by solving a scalar boundary value problem and it has two components: one responsible for driving the gripper toward the desired position and the other one responsible for guiding the gripper around obstacles. A detailed discussion of similarities and differences between these methods and the OVF method was presented by Rybus (2022).

The OVF method was validated in numerical simulations performed for a planar 2 Degrees of Freedom (DoF) manipulator mounted on a free-floating chaser satellite (Rybus, 2022). This method allows to obtain the desired position of the gripper, but it does not allow to obtain the desired orientation of the gripper. This is a major disadvantage as it is necessary to rotate the gripper to a specific orientation to perform the grasping manoeuvre (the gripper has to be fully aligned with a grasping interface on the non-cooperative target satellite).

In this paper, we introduce a modification to the OVF method that allows to obtain not only the desired position of the gripper, but also its desired orientation. We also investigate the possibility of application of the OVF method for a real system operating in microgravity conditions. As a case study, we consider a mock-up of a satellite-manipulator system operated on a planar air-bearing microgravity simulator. Such simulators are widely used for validation of trajectory planning and control algorithms in the field of space robotics (Rybus and Seweryn, 2016). Demonstration of the practical application of the OVF method for a system operating in simulated microgravity is the main contribution of this paper.

The paper is organised as follows. The dynamic equations of a satellite-manipulator system are presented in Section 2. The modified OVF method is described in Section 3. The obtained results are presented in Section 4 and discussed in Section 5. The conclusions are given in Section 6.

## 2. DYNAMICS OF THE FREE-FLOATING SATELLITE-MANIPULATOR SYSTEM

To describe the dynamics of a chaser satellite equipped with a manipulator, we follow the approach based on the Generalised Jacobian Matrix (Umetani and Yoshida, 1989). General equations that describe the dynamics of a satellite-manipulator system were presented by Seweryn and Banaszekiewicz (2008) and by Rybus et al. (2022). In this paper, we present application of these equations to a specific case: mock-up of a satellite-manipulator system operated on the planar air-bearing microgravity simulator at the Space Research Centre of the Polish Academy of Sciences (Basmadji et al., 2019). The mock-up of the chaser satellite is equipped with a 3 DoF manipulator. This system is shown in Figure 1. All joints of the manipulator are rotational.

We use the following vector of generalised coordinates (Junkins and Schaub, 1997):

$$\mathbf{q}_p = [\mathbf{r}_{ch}^T \quad \psi_{ch} \quad \boldsymbol{\theta}^T]^T, \quad (1)$$

where  $\mathbf{r}_{ch} = [r_{x_{ch}} \quad r_{y_{ch}}]^T$ ,  $r_{x_{ch}}$  and  $r_{y_{ch}}$  are the X and Y components of the chaser satellite centre of mass (CoM) position in the inertial frame of reference ( $\Pi_{ine}$ ), respectively,  $\psi_{ch}$  is the orientation of the chaser satellite,  $\boldsymbol{\theta} = [\theta_1 \quad \theta_2 \quad \theta_3]^T$ , while  $\theta_i$  is the angular position of the  $i$ -th joint. The vector of generalised velocities is given by

$$\mathbf{q}_v = [\mathbf{v}_{ch}^T \quad \omega_{ch} \quad \dot{\boldsymbol{\theta}}^T]^T, \quad (2)$$

where  $\mathbf{v}_{ch} = [v_{xch} \quad v_{ych}]^T$ ,  $v_{xch}$  and  $v_{ych}$  are the X and Y components of the chaser satellite CoM velocity, respectively,  $\omega_s$  is the angular velocity of the satellite, while  $\dot{\boldsymbol{\theta}}$  denotes the vector of angular velocities of manipulator joints.

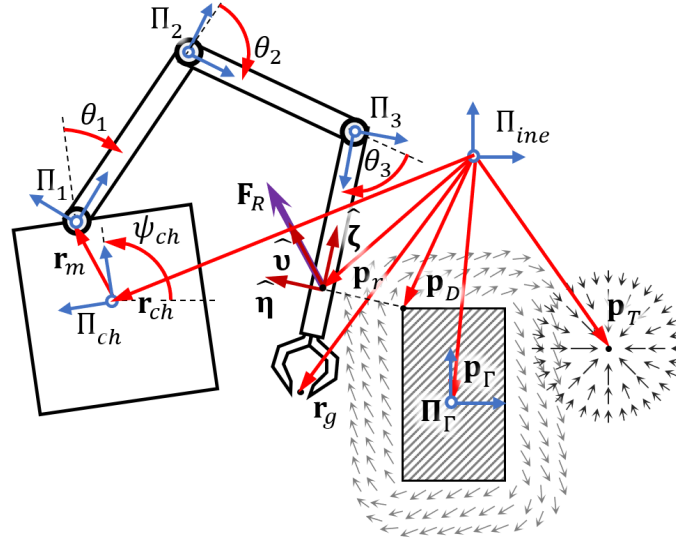


**Figure 1.** Schematic view of the free-floating satellite-manipulator system and the general idea of the OVF method

The state of the chaser satellite equipped with a manipulator is described by the following vector:

$$\mathbf{x} = [\mathbf{q}_v^T \quad \mathbf{q}_p^T]^T. \quad (3)$$

The dynamic equations of motion have the following form:

$$\dot{\mathbf{x}} = \begin{bmatrix} \mathbf{M}^{-1}(\mathbf{Q} - \mathbf{C}\mathbf{q}_v) \\ \mathbf{q}_v \end{bmatrix}, \quad (4)$$

where  $\mathbf{M}$  is the generalised inertia matrix and  $\mathbf{C}$  is the Coriolis matrix, while  $\mathbf{Q}$  denotes the vector of generalised forces:

$$\mathbf{Q} = [\mathbf{F}_{ch}^T \quad \tau_{ch} \quad \boldsymbol{\tau}_m^T]^T, \quad (5)$$

where  $\mathbf{F}_{ch} = [F_{xch} \quad F_{ych}]^T$ ,  $F_{xch}$  and  $F_{ych}$  are the X and Y components of external force acting on the chaser CoM, respectively,  $\tau_{ch}$  is the external torque acting on the satellite,  $\boldsymbol{\tau}_m = [\tau_1 \quad \tau_2 \quad \tau_3]^T$ , while  $\tau_i$  denotes the control torque applied at the  $i$ -th joint. Matrices  $\mathbf{M}$  and  $\mathbf{C}$  in (4) can be presented as

$$\mathbf{M} = \begin{bmatrix} \mathbf{M}_{ch} & \mathbf{M}_{ch/m} \\ \mathbf{M}_{ch/m}^T & \mathbf{M}_m \end{bmatrix}, \quad \mathbf{C} = \begin{bmatrix} \mathbf{C}_{ch} \\ \mathbf{C}_m \end{bmatrix}, \quad (6)$$

where  $\mathbf{M}_{ch}$  is the inertia matrix of the chaser satellite,  $\mathbf{M}_m$  is the inertia matrix of the manipulator,  $\mathbf{M}_{ch/m}$  is the inertia matrix that couples the chaser satellite with the manipulator,  $\mathbf{C}_{ch}$  is the Coriolis matrix of the chaser satellite, while  $\mathbf{C}_m$  is the Coriolis matrix of the manipulator. Definitions of  $\mathbf{M}_{ch}$ ,  $\mathbf{M}_m$ ,  $\mathbf{M}_{ch/m}$ ,  $\mathbf{C}_{ch}$  and  $\mathbf{C}_m$  matrices were presented by Rybus et al. (2022). In the considered case, the inertia matrix  $\mathbf{M}$  is non-singular and invertible.

Equation (4) describes the dynamic coupling between the manipulator and the chaser satellite (Xu, 1993).

The planar air-bearing microgravity simulator is used to emulate microgravity conditions. It provides frictionless motion of the system, hence the influence of external forces can be neglected (Rybus et al., 2019). No gravity acceleration is acting on the system in its plane of motion. The cold gas thrusters are mounted on the chaser satellite (Kindracki et al., 2017), but in the considered scenario, they are not used during the motion of the manipulator. Thus, we assume that  $F_{x_{ch}} = F_{y_{ch}} = \tau_{ch} = 0$ . In such a case, the momentum and the angular momentum of the system are conserved and equal to zero. The system is in a free-floating state, and changes in the position and orientation of the chaser satellite are caused by the manipulator motion (Dubowsky and Papadopoulos, 1993). The position of the CoM of the satellite-manipulator system remains stationary during the manipulator motion. Chaser satellite equipped with a manipulator is a nonholonomic system (Ratajczak and Tchoń, 2020).

The gripper is located at the end of the last link of the manipulator and its position in  $\Pi_{ine}$  is given by

$$\mathbf{r}_g = \begin{bmatrix} r_{x_g} \\ r_{y_g} \end{bmatrix} = \mathbf{r}_{ch} + \mathbf{R}_{ch} \mathbf{r}_m^{(\Pi_{ch})} + \sum_{i=1}^3 \mathbf{R}_i \mathbf{l}_i^{(\Pi_i)}, \quad (7)$$

where  $\mathbf{r}_m$  is the position of  $\Pi_1$  (the manipulator mounting point) with respect to the satellite CoM,  $\mathbf{l}_i$  is the position of the  $(i + 1)$ -th manipulator joint with respect to the  $i$ -th joint, and  $\mathbf{R}_{ch}$  and  $\mathbf{R}_i$  are the 2D rotation matrices (defined with respect to  $\Pi_{ine}$ ) of the chaser satellite and the  $i$ -th joint, respectively. The superscript in brackets denotes the frame of reference in which the vector is expressed. Vectors are expressed in the inertial frame  $\Pi_{ine}$  unless stated otherwise. The origin of  $\Pi_{ine}$  can be located in any arbitrarily selected position (the position of the CoM of the satellite-manipulator system is constant with respect to  $\Pi_{ine}$ ). In the considered planar case, the orientation of the gripper is expressed by

$$\psi_g = \psi_{ch} + \sum_{i=1}^3 \theta_i. \quad (8)$$

By differentiating (7) and (8) with respect to time, we obtain the expressions for the gripper linear and angular velocity,  $\mathbf{v}_g$  and  $\omega_g$ , respectively. These expressions can be presented as

$$\begin{bmatrix} \mathbf{v}_g \\ \omega_g \end{bmatrix} = \mathbf{J}_{ch} \begin{bmatrix} \mathbf{v}_{ch} \\ \omega_{ch} \end{bmatrix} + \mathbf{J}_m \dot{\boldsymbol{\theta}}, \quad (9)$$

where  $\mathbf{J}_{ch}$  is the Jacobian of the chaser satellite, while  $\mathbf{J}_m$  is the standard Jacobian of the fixed-base manipulator. Taking into account the assumption of zero momentum and angular momentum, we can present the following relationship between the velocities of manipulator joints and the velocity of the gripper:

$$\dot{\boldsymbol{\theta}} = \mathbf{J}_D^{-1} \begin{bmatrix} \mathbf{v}_g \\ \omega_g \end{bmatrix}, \quad (10)$$

where  $\mathbf{J}_D$  is the Dynamic Jacobian of the manipulator ( $3 \times 3$  matrix). This Jacobian takes into account the influence of the manipulator motion on the state of the satellite (Yoshida, 1994).

### 3. THE OVF METHOD

#### 3.1. Problem definition

The general idea of the OVF method is presented in Figure 1. To perform grasping of a non-cooperative target satellite, the gripper mounted on the manipulator has to be moved to a specific position and orientation with respect to the target object. The goal of the trajectory planning is to find a trajectory of the manipulator that allows to obtain the desired position and orientation of the gripper ( $\mathbf{p}_T$  and  $\psi_T$ , respectively). During the approach phase, the manipulator has to avoid collisions with the elements of the target satellite. Elements of complex shape can be approximated by simple geometric objects. We are considering  $m$  rectangular obstacles:  $\Gamma_1, \Gamma_2, \dots, \Gamma_m$ . The position of the geometrical centre of the  $i$ -th obstacle is denoted by  $\mathbf{p}_{\Gamma_i}$ , while the orientation of this obstacle with respect to  $\Pi_{ine}$  is denoted by  $\alpha_i$ . Width and height of the  $i$ -th obstacle are denoted by  $w_i$  and  $h_i$ , respectively. For the purpose of collision detection, the manipulator links are treated as line segments. The width of the links can be taken into account by introducing safe zones around the obstacles.

#### 3.2. Attractive force and torque

In the approach proposed by Rybus (2022), the virtual attractive force is responsible for driving the gripper towards the desired position. Here, we propose a simple extension of the OVF method that allows to obtain both the desired gripper position and the desired gripper orientation. We follow the approach described by Elahres et al. (2021), and we introduce an attractive torque that acts on the last link of the manipulator and allows to obtain the desired orientation of the gripper. The virtual force and torque that act on the gripper are given by

$$\begin{bmatrix} \mathbf{F}_A \\ \tau_A \end{bmatrix} = \begin{cases} \begin{bmatrix} \mathbf{F}_a \\ \tau_a \end{bmatrix}, & \text{if } \forall i \in \{1, 2, \dots, m\}: d_i > d_a \vee \overline{\mathbf{r}_g \mathbf{p}_T} \cap \Gamma_i = \emptyset \\ \mathbf{0}, & \text{if } \exists i \in \{1, 2, \dots, m\}: d_i \leq d_a \wedge \overline{\mathbf{r}_g \mathbf{p}_T} \cap \Gamma_i \neq \emptyset \end{cases}, \quad (11)$$

where  $d_i = \|(\mathbf{p}_r)_i - (\mathbf{p}_D)_i\|$  is the closest distance between the manipulator and the  $i$ -th obstacle,  $(\mathbf{p}_r)_i$  denotes the point on the manipulator that is closest to the obstacle  $\Gamma_i$ ,  $(\mathbf{p}_D)_i$  denotes the point on the obstacle  $\Gamma_i$  that is closest to the manipulator,  $d_a$  is the threshold value of  $d_i$  and  $\overline{\mathbf{r}_g \mathbf{p}_T}$  denotes the line segment between the current and the desired positions of the gripper. A simple algorithm that calculates distances between the line segments defined by the positions of manipulator kinematic pairs and sides of rectangular obstacles is used to find  $(\mathbf{p}_r)_i$  and  $(\mathbf{p}_D)_i$ . The  $\mathbf{F}_A$  and  $\tau_A$  are equal to zero if for any obstacle  $\Gamma_i$  the distance  $d_i$  is smaller than  $d_a$  and if this obstacle intersects with the line segment  $\overline{\mathbf{r}_g \mathbf{p}_T}$  (intersection occurs when there is a non-empty set of points that belong to the line segment  $\overline{\mathbf{r}_g \mathbf{p}_T}$  and to the obstacle  $\Gamma_i$ ).  $\mathbf{F}_a$  and  $\tau_a$  are given by the following expressions:

$$\mathbf{F}_a = g_{A1} (e^{-g_{A2} \|\mathbf{p}_T - \mathbf{r}_g\|} + g_{A3}) \frac{\mathbf{p}_T - \mathbf{r}_g}{\|\mathbf{p}_T - \mathbf{r}_g\|}, \quad (12)$$

$$\tau_a = g_{A1} (e^{-g_{A4} \|\psi_T - \psi_g\|} + g_{A5}), \quad (13)$$

where  $g_{A1}, g_{A2}, g_{A3}, g_{A4}$  and  $g_{A5}$  are the constant coefficients that are used to tune the OVF algorithm. Equation (13) is a new element introduced in the OVF method. This equation allows to apply the OVF method in the considered scenario of the grasping manoeuvre. The value of  $\mathbf{F}_a$  depends on the distance between the desired position and the current position of the gripper, while the value of  $\tau_a$  depends on the difference between the current orientation and the desired orientation of the gripper. The idea that the amplitude of the attractive force

depends on the distance and should be determined using the exponential function was introduced by Volpe and Khosla (1987). In the OVF method, the coefficients in (12) and (13) are selected in such a way that the value of the attractive force is approximately constant when the gripper is far away from the desired position. As the gripper gets closer to the desired position, the value of the attracting force increases. This allows to find a solution of the trajectory planning problem even when the desired position is close to the surface of the obstacle. Moreover, the proposed approach allows to obtain very small final positioning error.

### 3.3. Repulsive force

In the OVF method, each obstacle generates a vector field. The repulsive force that acts on the manipulator results from the vector fields generated by multiple obstacles. Only the collisions between the manipulator links and external obstacles located in the manipulator workspace are taken into account. Self-collisions between the manipulator links and collisions between the manipulator links and the elements of the chaser satellite are not considered. The approach presented in this section is based on the original formulation of the OVF method described by Rybus (2022).

The vector field of the obstacle  $\Gamma_i$  is constructed from the potential field that surrounds this obstacle. The Force Impliquant une Répulsion Artificielle en Surface (FIRAS) potential function (Khatib, 1986) is used to calculate the value of the potential for the point  $(\mathbf{p}_r)_i$  (the point on the manipulator that is closest to the obstacle  $\Gamma_i$ ):

$$U_i = \begin{cases} u_i, & \text{if } 0 < \left\| (\mathbf{p}_r^{(\Gamma_i)})_i - (\mathbf{p}_D^{(\Gamma_i)})_i \right\| < d_0 \\ 0, & \text{otherwise} \end{cases}, \quad (14)$$

where the superscript  $(\Gamma_i)$  indicates that the position of the given point is expressed in  $\Pi_{\Gamma_i}$ , while  $d_0$  is a constant parameter that describes the effective range of the potential field.  $u_i$  is given by the following expression:

$$u_i = \frac{g_P}{2} \left( \frac{1}{\left\| (\mathbf{p}_r^{(\Gamma_i)})_i - (\mathbf{p}_D^{(\Gamma_i)})_i \right\|} - \frac{1}{d_0} \right)^2, \quad (15)$$

where  $g_P$  is a constant coefficient. To obtain the direction pointing away from the obstacle  $\Gamma_i$ , we calculate the gradient of the scalar potential field as follows:

$$\boldsymbol{\eta}_i = \nabla U_i. \quad (16)$$

The following expression is used to calculate the direction perpendicular to the gradient of the potential field:

$$\boldsymbol{\zeta}_i = \mathbf{T}_\gamma \left( \gamma_i \frac{\pi}{2} \right) \hat{\boldsymbol{\eta}}_i, \quad (17)$$

where the symbol  $\hat{\cdot}$  denotes the unit vector ( $\hat{\boldsymbol{\eta}}_i = \frac{\boldsymbol{\eta}_i}{\|\boldsymbol{\eta}_i\|}$ ),  $\mathbf{T}_\gamma$  is the 2D rotation matrix, while the parameter  $\gamma_i \in \{-1, 1\}$  defines the direction of the vector  $\boldsymbol{\zeta}_i$ . The selection of  $\gamma_i$  for given initial conditions and for a given set of obstacles depends on  $\mathbf{p}_T$ . Various combinations of  $\gamma_i$  must be checked to find the solution of the trajectory planning problem. The number of possible combinations depends on the number of obstacles and is equal to  $2^m$ . Values of  $\gamma_i$  coefficients in the  $z$ -th set are obtained with the following equation:

$$\gamma_i = (-1)^{\left\lfloor \frac{z+2^{i-1}-1}{2^{i-1}} \right\rfloor}, \quad (18)$$

where  $\lfloor \cdot \rfloor$  denotes the floor function. The resultant direction of the force is defined by the unit vector  $\hat{\mathbf{v}}_i$ , where  $\mathbf{v}_i$  is given by

$$\mathbf{v}_i = \begin{cases} \hat{\boldsymbol{\eta}}_i + g_h \hat{\boldsymbol{\zeta}}_i, & \text{if } \overline{\mathbf{r}_g \mathbf{p}_T} \cap \Gamma_i = \emptyset \\ \frac{-\tan^{-1}(g_w(d_i - d_v))}{0.5\pi} \hat{\boldsymbol{\eta}}_i + g_h \hat{\boldsymbol{\zeta}}_i, & \text{if } \overline{\mathbf{r}_g \mathbf{p}_T} \cap \Gamma_i \neq \emptyset \end{cases}, \quad (19)$$

where  $g_w$  and  $g_h$  are constant coefficients, while  $d_v$  is a constant parameter that describes the distance from the obstacle at which  $\mathbf{v}_i$  changes its direction.

If the  $i$ -th obstacle does not lie between the current position of the gripper and the desired position (the set of points belonging to the line segment  $\overline{\mathbf{r}_g \mathbf{p}_T}$  and to the obstacle  $\Gamma_i$  is empty), then  $\mathbf{v}_i$  is calculated as a sum of vectors  $\hat{\boldsymbol{\eta}}_i$  (vector defined by the gradient of the potential field) and  $\hat{\boldsymbol{\zeta}}_i$  (vector parallel to the lines of the potential field). Vector  $\hat{\boldsymbol{\zeta}}_i$  is multiplied by a weight coefficient  $g_h$  which influences the direction of  $\mathbf{v}_i$  (low value of  $g_h$  results in a direction that points away from the obstacle, while high values result in a direction that moves the manipulator around the obstacle). If the gripper is in close proximity to the obstacle that lies between the gripper and the desired position, then the manipulator motion results only from the vector field of that obstacle. In such a situation, the manipulator is guided around the obstacle at the defined distance (this is ensured by the first term of (19) under the condition that  $\overline{\mathbf{r}_g \mathbf{p}_T} \cap \Gamma_i \neq \emptyset$ ).

The  $i$ -th obstacle acts on the point on the manipulator that is closest to this obstacle,  $(\mathbf{p}_r)_i$ , with the virtual repulsive force

$$(\mathbf{F}_R)_i = g_{R1}(-e^{-g_{R2}\|\mathbf{p}_T - \mathbf{r}_g\|} + g_{R3})U_i \hat{\mathbf{v}}_i, \quad (20)$$

where  $g_{R1}$ ,  $g_{R2}$  and  $g_{R3}$  denote constant coefficients. The value of the repulsive force depends on the distance between the desired position and the current position of the gripper. The value of this force decreases as the distance decreases. The presented approach allows to plan a trajectory even if  $\mathbf{p}_T$  lies very close to the obstacle.

### 3.4. Trajectory planning

The motion of the manipulator is directed by the virtual attractive and repulsive forces. The following equation is used to calculate the desired motion of manipulator joints under the influence of these forces:

$$\dot{\boldsymbol{\theta}}_{des} = \mathbf{J}_D^{-1} g_v \begin{bmatrix} \mathbf{F}_A \\ \boldsymbol{\tau}_A \end{bmatrix} + \sum_{i=1}^m \mathbf{J}_{D_i}^{\#} g_v \mathbf{T}_\gamma(\varphi_i) (\mathbf{F}_R)_i, \quad (21)$$

where  $\dot{\boldsymbol{\theta}}_{des} = [\dot{\theta}_{1des} \quad \dot{\theta}_{2des} \quad \dot{\theta}_{3des}]^T$ ,  $\#$  denotes the Moore–Penrose pseudoinverse,  $g_v$  is a constant coefficient and  $\mathbf{J}_{D_i}$  is the Dynamic Jacobian computed for the point  $(\mathbf{p}_r)_i$ . This point may not lie on the last link of the manipulator, but on the  $j$ -th link. Thus, in the calculation of  $\mathbf{J}_{D_i}$ , only those joints are taken into account which are located between the manipulator mounting point and the link on which  $(\mathbf{p}_r)_i$  lies. In such a case, the position of  $(\mathbf{p}_r)_i$  is considered as an end point of the  $j$ -th link. Matrix  $\mathbf{T}_\gamma$  is used to transform  $(\mathbf{F}_R)_i$  from  $\Pi_{ine}$  to the local coordinate frame fixed at the beginning of the  $j$ -th link. Orientation of this link is denoted by  $\varphi_i$  (index  $i$  indicates that the considered link is closest to the  $i$ -th obstacle).

The control torques that result in the desired motion of the manipulator joints are calculated from the following equation:

$$\boldsymbol{\tau}_m = g_u (\dot{\boldsymbol{\theta}}_{des} - \dot{\boldsymbol{\theta}}), \quad (22)$$



where  $g_u$  is a constant coefficient. Equation (4) is solved with the fourth order Runge–Kutta (RK IV) method to determine the state of the system after the application of the control torque given by (22). Calculation of the attractive and repulsive forces is repeated for the new state obtained from the RK IV method. This process is continued until the gripper reaches the desired position and orientation or until the maximal number of repetitions is reached. As a result, we obtain the reference manipulator trajectory. The trajectory is smoothed and the distribution of the points that form the trajectory is changed with the method described by Rybus and Seweryn (2018). At this stage, the time of motion can be selected arbitrarily and the trajectory can be adjusted. Finally, we obtain the reference gripper position and orientation as a function of time:  $(\mathbf{r}_g(t))_{ref}, (\psi_g(t))_{ref}$ .

### 3.5. Closed-loop controller

To apply the OVF method on a real system, it is necessary to implement a closed-loop controller responsible for trajectory tracking. To control the gripper in the Cartesian space, we use the following control law:

$$\dot{\boldsymbol{\theta}} = \mathbf{J}_D^{-1} g_c \left( \begin{bmatrix} (\mathbf{r}_g)_{ref} \\ (\psi_g)_{ref} \end{bmatrix} - \begin{bmatrix} \mathbf{r}_g \\ \psi_g \end{bmatrix} \right). \quad (23)$$

The gripper position and orientation error are multiplied by a constant gain  $g_c$  to obtain the desired instantaneous velocity of the gripper. This velocity is multiplied by the inverse of the Dynamic Jacobian (this approach cannot be used when the manipulator is close to dynamic singularities). Proportional–Integral–Derivative (PID) controllers are responsible for tracking the joint positions obtained by integration of the joint velocities calculated from (23).

## 4. VALIDATION OF THE OVF METHOD

### 4.1. Test-bed description and parameters of the system

The practical application of the OVF method is demonstrated in experiments performed on the planar air-bearing microgravity simulator operated at the Space Research Centre of the Polish Academy of Sciences. This test-bed consists of a granite plate (2 m × 3 m). The plate is flat and precisely levelled. The mock-up of the chaser satellite is equipped with the 3 DoF planar manipulator. The mock-up and the manipulator are mounted on planar air-bearings that use a thin film of pressurised air to provide frictionless motion on the surface of the granite plate. The microgravity conditions are simulated in the horizontal plane. The air-bearings are supplied with air from a gas canister located on the chaser mock-up. The closed-loop control system is implemented on the main computer (ATSAMA5D36), which is also located on the chaser mock-up. Direct Current (DC) motors are used to drive the joints of the manipulator. Each joint is equipped with a harmonic drive and an absolute optical encoder. All actuators have separate drivers connected to a CAN-bus. External vision system is used to provide measurements of the gripper position and orientation in  $\Pi_{ine}$ . Detailed description of this test-bed was presented by Basmadji et al. (2019). The mass of the chaser satellite is: 58.69 kg, while its mass moment of inertia is: 2.418 kg · m<sup>2</sup>. The position of the manipulator mounting point with respect to the chaser CoM is  $\mathbf{r}_m^{(\Pi_{ch})} = [0.377 \text{ m} \quad -0.001 \text{ m}]^T$ . Properties of the manipulator are given in Table 1. Inertia properties of the satellite and the manipulator were obtained before the test campaign with the use of a simple identification procedure.

**Table 1.** Mass and geometrical properties of the manipulator

Parameter	Unit	Link 1	Link 2	Link 3
Length	m	0.45	0.45	0.31
Mass	kg	2.81	2.82	4.64
CoM position in $\Pi_i$	m	$\begin{bmatrix} 0.136 \\ -0.002 \end{bmatrix}$	$\begin{bmatrix} 0.134 \\ -0.001 \end{bmatrix}$	$\begin{bmatrix} 0.151 \\ 0 \end{bmatrix}$
Mass moment of inertia	$\text{kg} \cdot \text{m}^2$	0.0637	0.0635	0.0515

## 4.2. Scenario definition

The following scenario was selected for demonstration of the OVF method. The origin of  $\Pi_{ine}$  is located on the test-bed surface in a position that coincides with the origin of the coordinate frame of the external vision system used in the experiments. The initial position of the chaser satellite CoM is  $r_{x_{ch}}(t=0) = 0.2$  m and  $r_{y_{ch}}(t=0) = 0.7$  m, while the initial orientation of the chaser is  $\psi_{ch}(t=0) = 0$ . The initial configuration of the manipulator is defined as  $\theta_1(t=0) = 80.50^\circ$ ,  $\theta_2(t=0) = -119.51^\circ$  and  $\theta_3(t=0) = -51.00^\circ$ . For this initial configuration of the system, we obtain the following position and orientation of the gripper:  $r_{x_g}(t=0) = 1.00$  m,  $r_{y_g}(t=0) = 0.55$  m and  $\psi_g(t=0) = -90^\circ$ . In the considered scenario, there is one rectangular obstacle located inside the manipulator workspace. The centre of the obstacle  $\Gamma_1$  is in  $\mathbf{p}_{\Gamma_1} = [1.2 \text{ m} \ 0.55 \text{ m}]^T$ . The edges of this obstacle are parallel to the axes of  $\Pi_{ine}$  and have the following lengths:  $w_1 = 0.12$  m and  $h_1 = 0.22$  m. The obstacle  $\Gamma_1$  represents an element of the non-cooperative target satellite. The gripper has to reach the desired grasping point located on the opposite side of the obstacle  $\Gamma_1$ :  $\mathbf{p}_T = [r_{x_g}(t=t_f) \ r_{y_g}(t=t_f)]^T = [1.35 \text{ m} \ 0.55 \text{ m}]^T$ . To perform the grasping operation, the gripper has to reach the following final orientation:  $\psi_T = \psi_g(t=t_f) = -90^\circ$ . The time allocated for realisation of the trajectory is arbitrarily set to  $t_f = 16$  s.

Values of the parameters and the constant coefficients in the OVF method were selected by a trial and error method for the given parameters of the system. The following values were used to solve the presented trajectory planning problem:  $g_{A1} = 100$ ,  $g_{A2} = 70$ ,  $g_{A3} = 2.5$ ,  $g_{A4} = 70$ ,  $g_{A5} = 2.5$ ,  $d_a = 0.1$  m,  $g_p = 0.005$ ,  $d_0 = 10$  m,  $g_w = 10^4$ ,  $g_h = 1.5$ ,  $d_v = 0.02$  m,  $g_{R1} = 5$ ,  $g_{R2} = 50$ ,  $g_{R3} = 1$ ,  $g_v = 1$ ,  $g_u = 3.125$ . Trajectory planning was performed offline before the beginning of the experiments. Laptop with Intel Core i7-10510U CPU (2.30 GHz) and 16 GB RAM was used for this purpose.

## 4.3. Results of experiments

The test campaign on the planar air-bearing microgravity simulator consisted of 10 repetitions of the experiment. No real obstacle was used in experiments to avoid the risk of a collision in case of problems with the proper realisation of the planned trajectory. The results of six experiments were selected for further analysis and are presented in this section, while the results of four experiments were rejected due to the occurrence of large external disturbances or problems with data recording. The reference gripper trajectory planned with the OVF method and the trajectories obtained in the experiments are shown in Figure 2 on the XY plane. The X and Y components of the gripper position are shown in Figure 3, where the reference position and the desired position (that corresponds to the position of the selected grasping point) are also presented. The orientation of the gripper is shown on the left panel of Figure 4, while the orientation of the chaser satellite mock-up is shown on the right panel of

Figure 4. The angular positions of the manipulator joints measured with encoders during the experiments are presented in Figure 5. These positions are compared with the positions obtained in simulations performed for the reference gripper trajectory. Frames captured by the camera of the external vision system are shown in Figure 6. This camera is mounted above the surface of the granite table. Gripper final positioning errors obtained in numerical simulations for the reference trajectory and in the experiments performed on the air-bearing microgravity simulator are presented in Table 2.

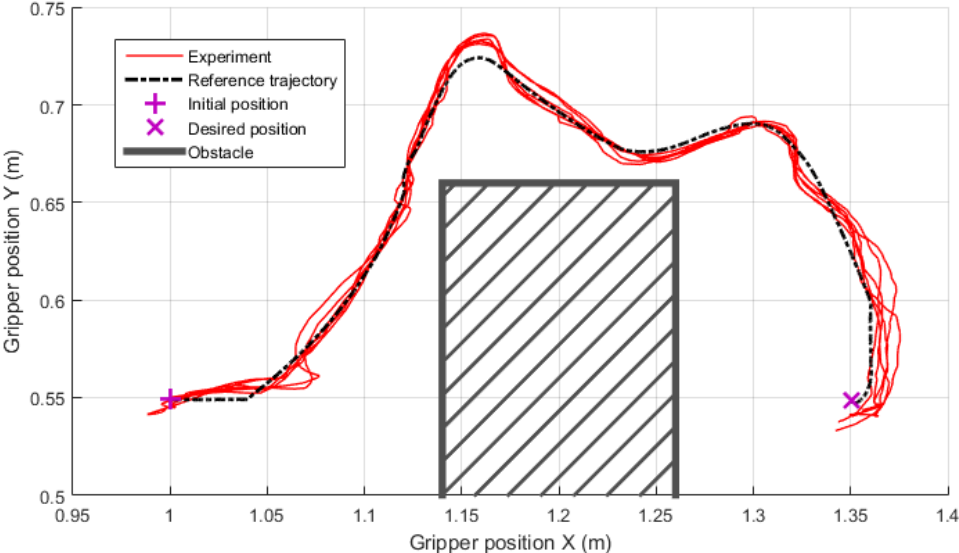


Figure 2. Gripper trajectory on the XY plane

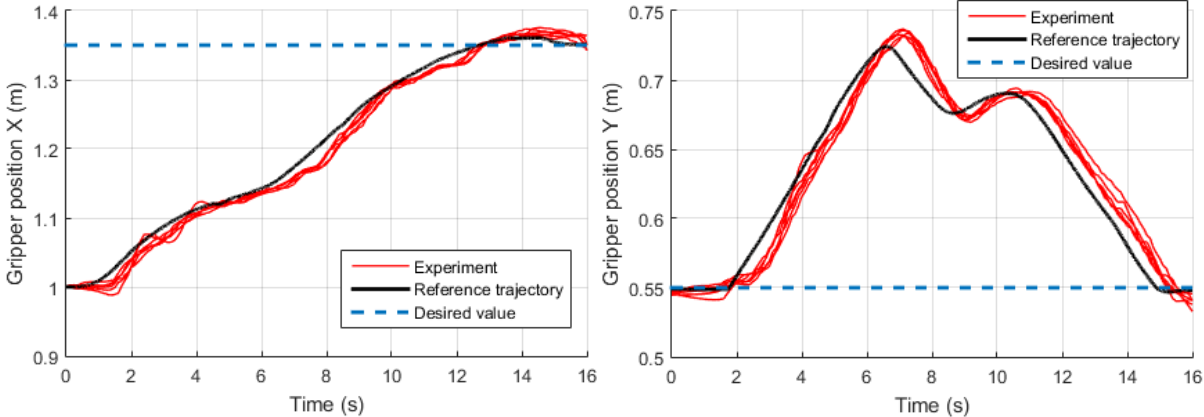
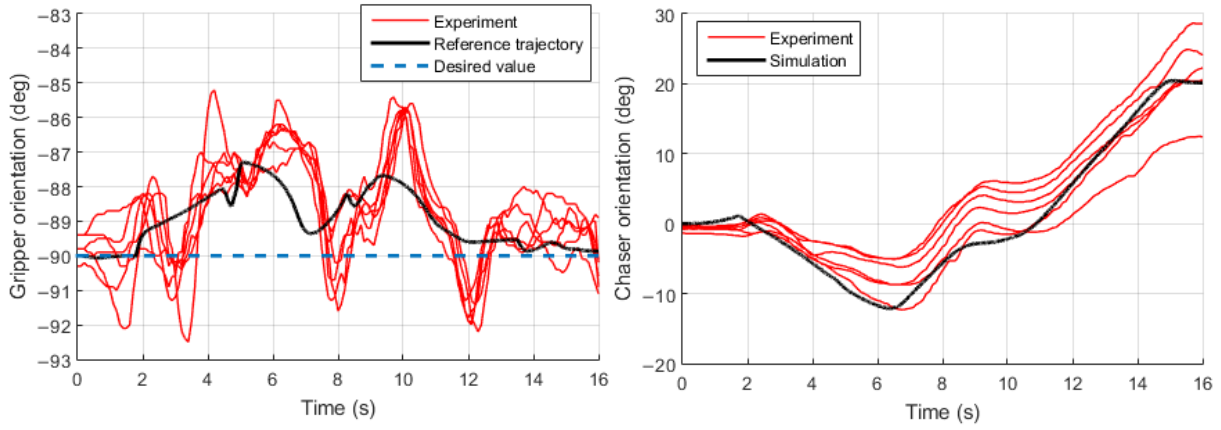
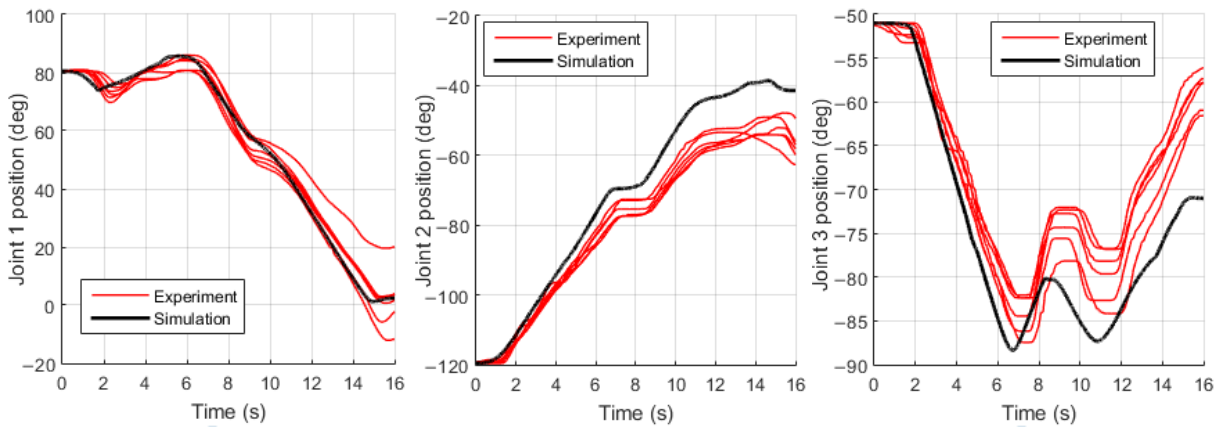


Figure 3. Gripper position: X component (left) and Y component (right)



**Figure 4.** Gripper orientation (left) and chaser satellite orientation (right)



**Figure 5.** Angular positions of manipulator joints

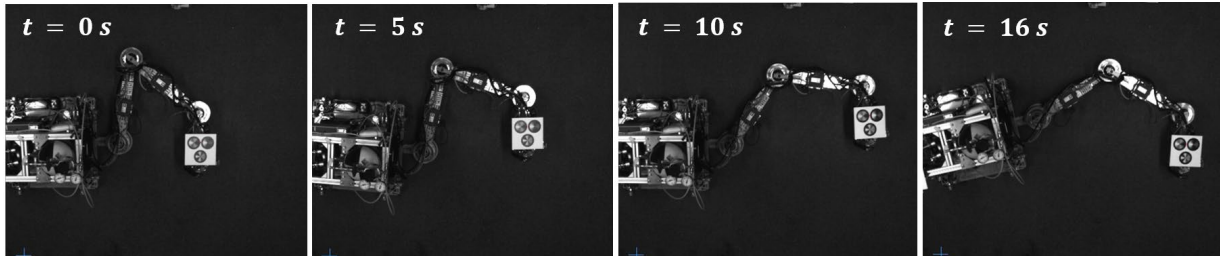


**Figure 6.** Chaser satellite mock-up equipped with the 3 DoF manipulator during one of the experiments

**Table 2.** Gripper final positioning errors (absolute values)

Parameter	Unit	Reference (planning)	Experiments		
			Min.	Max.	Average
Position X	m	0.0008	0.0005	0.0078	0.0043
Position Y	m	0.0018	0.0064	0.0171	0.0106
Orientation	deg	0.1319	0.0999	1.2999	0.5666

## 5. DISCUSSION

The OVF method was able to find the collision-free trajectory in the given scenario. As demonstrated by Rybus (2022), the proposed method is able to solve difficult trajectory planning problems. The selected set of parameters and constant coefficients should allow successful planning in a wide range of conditions. However, there is no simple method and no automatic algorithm for selecting the values of parameters and coefficients in the OVF method. The process of selecting these values using the trial and error method is tedious and lengthy. Finding a collision-free trajectory in a different scenario may require a different set of values. This is a disadvantage of the proposed approach. Moreover, if the solution exists for a given problem, it is not guaranteed that the OVF method will be able to find this solution. In very difficult scenarios, the OVF method and other methods based on potential fields may fail to find a solution due to the fact that the considered system is nonholonomic. In such scenarios, other methods should be used, for example, the RRT algorithm (Rybus, 2020). However, the time required by the RRT method is much longer than the time required by the OVF method (Rybus, 2022).

The reference gripper trajectory obtained with the OVF method in the considered scenario is smooth. The results of the test campaign confirm that the OVF method can be successfully applied for a real system operating in simulated microgravity conditions. As it is evident from Figure 3 and from the left panel of Figure 4, the gripper closely followed the reference trajectory. The closed-loop controller implemented on the chaser satellite on-board computer was able to ensure satisfactory trajectory tracking despite disturbances acting on the system (e.g. force resulting from non-perfect levelling of the granite plate). The delay in the trajectory tracking in the Cartesian space results from the application of a simple proportional control law. The maximal position and orientation errors at the end of the trajectory (Table 2) are small and fall within the tolerance of the gripper. Thus, in every experiment, the gripper reached the position and orientation that would allow to perform a successful capture operation. In none of the experiments, the links of the manipulator moved through the area occupied by the obstacle. Thus, no collision would occur in experiments.

The trajectory tracking was performed in the Cartesian space, and closed-loop controller was compensating the gripper position and orientation errors. Thus, due to disturbances acting on the system, there are moderate differences between the manipulator trajectories in the joint space obtained in individual experiments (Figure 5). The positions of the manipulator joints obtained in the experiments and the positions obtained in the numerical simulation performed for the reference gripper trajectory also differ, but these differences are expected (the system was not following the trajectory defined in the joint space).

The influence of the manipulator motion on the position and orientation of the chaser satellite mock-up is clearly visible in Figure 6. Moderate differences between the chaser satellite mock-up orientation obtained in individual experiments result from the disturbances and from the fact that the trajectories in the joint space were different. The changes of the chaser satellite mock-up orientation measured in the experiments are relatively close to the changes of the orientation obtained in numerical simulations performed for the reference gripper trajectory (the right panel of Figure 4). As the satellite-manipulator system was free-floating, these results show the correctness of the system modelling and the identification of its parameters.

The further development of the OVF method will focus on extending the presented approach to a spatial (three-dimensional) case, in which the motion of the system is not limited to one plane. The three-dimensional case is much more complex, as the chaser satellite could rotate around any axis and its orientation should be described by Euler angles or quaternions. In this

case, a three-element vector would describe the desired position of the gripper, while another three-element vector would describe its desired orientation. The vector field would have to be constructed in three dimensions and additional parameters would be required to describe this field. It is also planned to take into account the possibility of self-collisions between the manipulator links. Additional scenarios will be considered to better evaluate the performance of the proposed method.

## 6. CONCLUSIONS

The OVF method takes into account the fact that in the microgravity conditions, the state of the satellite is influenced by the motion of the manipulator. The dynamic equations of the satellite-manipulator system are used during trajectory planning. The OVF method can be applied to plan a collision-free trajectory of a manipulator in difficult scenarios. The modified version of the OVF method presented in this paper allows to obtain the desired position and orientation of the gripper. To perform the grasping manoeuvre, the gripper has to be positioned in a specific point and aligned with the grasping interface. Thus, the modification introduced in the OVF method allows this method to be applied in the planned ADR missions. The OVF method was used to plan a collision-free trajectory of a 3 DoF manipulator mounted on a chaser satellite mock-up. The practical applicability of the presented method was successfully demonstrated in the experiments performed in simulated microgravity conditions. The gripper followed the reference trajectory despite disturbances acting on the system. The final position and orientation of the gripper obtained in experiments were close to the desired position and orientation required for the capture operation. The OVF method may not be able to find the solution of the trajectory planning problem in some very difficult scenarios. However, this method requires less computational time than the RRT algorithm. Moreover, unlike the RRT algorithm, the OVF method is fully deterministic and it will always produce the same result. This is an important issue when assessing the possibility of the practical application of the OVF method in the future orbital missions.

**Acknowledgements.** This paper was partially supported by the Polish National Centre for Research and Development project no. LIDER/19/0117/L-10/18/NCBR/2019.

## REFERENCES

- Basmadji F.L., Chmaj G., Rybus T., Seweryn K. (2019) Microgravity testbed for the development of space robot control systems and the demonstration of orbital maneuvers, *Proceedings of SPIE: Photonics Applications in Astronomy, Communications, Industry, and High-Energy Physics Experiments*, 111763V, Wilga, Poland.
- Benevides J.R., Grassi V. (2015) Autonomous path planning of free-floating manipulators using RRT-based algorithms, *Proc. 12th Latin American Robotics Symposium and 3rd Brazilian Symposium on Robotics (LARS-SBR)*, Uberlandia, Minas Gerais, Brazil, 139-144.
- Biesbroek R., Innocenti L., Wolahan A., Serrano S.M. (2017) e. Deorbit – ESA’s active debris removal mission, *Proc. 7th European Conference on Space Debris*, Darmstadt, Germany.
- Biesbroek R., Aziz S., Wolahan A., Cipolla S., Richard-Noca M., Piguet L. (2021) The Clearspace-1 mission: ESA and Clearspace team up to remove debris, *Proc. 8th European Conference on Space Debris*, Darmstadt, Germany.
- Bonnal C., Ruault J.M., Desjean M.C. (2013) Active debris removal: Recent progress and current trends, *Acta Astronautica*, Vol. 85, 51-60.

- Dubowsky S., Papadopoulos E. (1993) The kinematics, dynamics, and control of free-flying and free-floating space robotic systems, *IEEE Transactions on Robotics and Automation*, Vol. 9, No. 5, 531-543.
- Elahres M., Fonte A., Poisson G. (2021) Evaluation of an artificial potential field method in collision-free path planning for a robot manipulator, *Proc. 2nd International Conference on Robotics, Computer Vision and Intelligent Systems*, Valletta, Malta, 92-102.
- Estable S., Pruvost C., Ferreira E., Telaar J., Fruhnert M., et al. (2020) Capturing and deorbiting Envisat with an Airbus Spacetug. Results from the ESA e.deorbit Consolidation Phase study, *Journal of Space Safety Engineering*, Vol. 7, No. 1, 52-66.
- Flores-Abad A., Ma O., Pham K., Ulrich S. (2014) A review of space robotics technologies for on-orbit servicing, *Progress in Aerospace Sciences*, Vol. 68, 1-26.
- Gao X., Jia Q., Sun H., Chen G. (2011) Research on path planning for 7-DOF space manipulator to avoid obstacle based on A\* algorithm, *Sensor Letters*, Vol. 9, No. 4, 1515-1519.
- Junkins J.L., Schaub H. (1997) An instantaneous eigenstructure quasivelocity formulation for nonlinear multibody dynamics, *The Journal of the Astronautical Sciences*, Vol. 45, No. 3, 279-295.
- Khatib O. (1986) The potential field approach and operational space formulation in robot control, In: Narendra K.S. (ed.), *Adaptive and Learning Systems*, Springer, Boston, 367-377.
- Kindracki J., Tur K., Paszkiewicz P., Mężyk Ł., Boruc Ł., Wolański P. (2017) Experimental research on low-cost cold gas propulsion for a space robot platform, *Aerospace Science and Technology*, Vol. 62, 148-157.
- Kowalczyk W., Michałek M., Kozłowski K. (2012) Trajectory tracking control with obstacle avoidance capability for unicycle-like mobile robot, *Bulletin of the Polish Academy of Sciences: Technical Sciences*, Vol. 60, No. 3, 537-546.
- Lin C.C., Chuang J.H. (2003) Potential-based path planning for robot manipulators in 3-D workspace, *Proc. IEEE International Conference on Robotics and Automation (ICRA'2003)*, Taipei, Taiwan, vol. 3, 3353-3358.
- Liou J.C., Johnson N.L., Hill N.M. (2010) Controlling the growth of future LEO debris populations with active debris removal, *Acta Astronautica*, Vol. 66, No. 5-6, 648-653.
- Masoud A.A., Al-Shaikhi A. (2015) Time-sensitive, sensor-based, joint planning and control of mobile robots in cluttered spaces: A harmonic potential approach, *Proc. 54th IEEE Conference on Decision and Control (CDC'2015)*, Osaka, Japan, 2761-2766.
- Masoud A.A., Bayoumi M.M. (1993) Robot navigation using the vector potential approach, *Proc. IEEE International Conference on Robotics and Automation (ICRA'1993)*, Atlanta, GA, USA, vol. 1, 805-811.
- Misra G., Bai X. (2017) Optimal path planning for free-flying space manipulators via sequential convex programming, *Journal of Guidance, Control, and Dynamics*, Vol. 40, No. 11, 3019-3026.
- Mukherjee R., Nakamura Y. (1991) Nonholonomic redundancy of space robots and its utilization via hierarchical liapunov functions, *Proc. American Control Conference (ACC'1991)*, Boston, USA, 1491-1496.
- Murtaza A., Pirzada S.J.H., Xu T., Jianwei L. (2020) Orbital debris threat for space sustainability and way forward, *IEEE Access*, Vol. 8, 61000-61019.

- Pamosoaji A.K., Hong K.S. (2013) A path-planning algorithm using vector potential functions in triangular regions, *IEEE Transactions on Systems, Man, and Cybernetics: Systems*, Vol. 43, No. 4, 832-842.
- Park M.G., Lee M.C. (2003) A new technique to escape local minimum in artificial potential field based path planning, *KSME International Journal*, Vol. 17, 1876-1885.
- Ratajczak J., Tchoń K. (2020) Normal forms and singularities of non-holonomic robotic systems: A study of free-floating space robots, *Systems and Control Letters*, Vol. 138, 104661.
- Rybus T. (2018) Obstacle avoidance in space robotics: Review of major challenges and proposed solutions, *Progress in Aerospace Sciences*, Vol. 101, 31-48.
- Rybus T. (2020) Point-to-point motion planning of a free-floating space manipulator using the Rapidly-exploring Random Trees (RRT) method, *Robotica*, Vol. 38, No. 6, 957-982.
- Rybus T. (2022) The Obstacle Vector Field (OVF) method for collision-free trajectory planning of free-floating space manipulator, *Bulletin of the Polish Academy of Sciences: Technical Sciences*, Vol. 70, No. 2, e140691.
- Rybus T., Seweryn K. (2016) Planar air-bearing microgravity simulators: review of applications, existing solutions and design parameters, *Acta Astronautica*, Vol. 120, 239-259.
- Rybus T., Seweryn K. (2018) Zastosowanie metody sztucznych pól potencjału do planowania trajektorii manipulatora satelitarnego [in polish: Application of the artificial potential field method for trajectory planning of space manipulator], In: Tchoń K., Zieliński C. (eds.), *Prace Naukowe Politechniki Warszawskiej: Elektronika*, Vol. 196, Oficyna Wydawnicza Politechniki Warszawskiej, Warszawa, 61-74.
- Rybus T., Wojtunik M., Basmadji F.L. (2022) Optimal collision-free path planning of a free-floating space robot using spline-based trajectories, *Acta Astronautica*, Vol. 190, 395-408.
- Rybus T., Seweryn K., Oleś J., Basmadji F.L., Tarenko K., Moczydłowski R., Barciński T., Kindracki J., Mężyk Ł., Paszkiewicz P., Wolański P. (2019) Application of a planar air-bearing microgravity simulator for demonstration of operations required for an orbital capture with a manipulator, *Acta Astronautica*, Vol. 155, 211-229.
- Seweryn K., Banaszkiwicz M. (2008) Optimization of the trajectory of a general free-flying manipulator during the rendezvous maneuver, *Proc. AIAA Guidance, Navigation, and Control Conference and Exhibit (AIAA-GNC'2008)*, Honolulu, HI, USA.
- Shan M., Guo J., Gill E. (2016) Review and comparison of active space debris capturing and removal methods, *Progress in Aerospace Sciences*, Vol. 80, 18-32.
- Umetani Y., Yoshida K. (1989) Resolved motion rate control of space manipulators with generalized Jacobian matrix, *IEEE Transactions on Robotics and Automation*, Vol. 5, No. 3, 303-314.
- Volpe R., Khosla P. (1987) Artificial potentials with elliptical isopotential contours for obstacle avoidance, *Proc. 26th IEEE Conference on Decision and Control (CDC'1987)*, Los Angeles, CA, USA, 180-185.
- Wang M., Luo J., Fang J., Yuan J. (2018) Optimal trajectory planning of free-floating space manipulator using differential evolution algorithm, *Advances in Space Research*, Vol. 61, No. 6, 1525-1536.



Xu Y. (1993) The measure of dynamic coupling of space robot systems, *Proc. IEEE International Conference on Robotics and Automation (ICRA'1993)*, Atlanta, GA, USA, vol. 3, 615-620.

Yanoshita Y., Tsuda S. (2009) Space Robot Path Planning for Collision Avoidance, *Proc. International MultiConference of Engineers and Computer Scientists (IMECS'2009)*, Hong Kong.

Yoshida K. (1994) Space robotics research activity with Experimental Free-Floating Robot Satellite (EFFORTS) simulators, In: Yoshikawa, T. and Miyazaki, F. (eds.), *Experimental Robotics III. Lecture Notes in Control and Information Sciences*, Vol. 200. Springer, Berlin, Heidelberg, 561-578.

**Received:** 2022-12-14

**Reviewed:** 2023-02-08 (undisclosed name); 2023-04-16 (E. Jarzębowska)

**Accepted:** 2023-05-23